THE JOURNAL OF BIOLOGICAL CHEMISTRY VOL. 290, NO. 28, pp. 17535–17545, July 10, 2015

Channel Gating Dependence on Pore Lining Helix Glycine Residues in Skeletal Muscle Ryanodine Receptor*

Received for publication, April 17, 2015, and in revised form, May 12, 2015 Published, JBC Papers in Press, May 21, 2015, DOI 10.1074/jbc.M115.659672

Yingwu Mei[1], Le Xu, David D. Mowrey, Raul Mendez Giraldez[2], Ying Wang[3], Daniel A. Pasek, Nikolay V. Dokholyan[4], and Gerhard Meissner[4,5]

From the Department of Biochemistry and Biophysics, University of North Carolina, Chapel Hill, North Carolina 27599

Background: Skeletal muscle ryanodine receptor (RyR1) releases Ca^{2+} ions from sarcoplasmic reticulum through Ca^{2+}-gated ion channels.
Results: Mutagenesis of two glycine residues in the pore-lining helix altered channel gating and ion conductance.
Conclusion: Pore-lining helix glycines provide flexibility and minimize clashes between amino acid residues.
Significance: Pore-lining helix glycines expedite channel gating by RyR1.

Type 1 ryanodine receptors (RyR1s) release Ca^{2+} from the sarcoplasmic reticulum to initiate skeletal muscle contraction. The role of RyR1-G4934 and -G4941 in the pore-lining helix in channel gating and ion permeation was probed by replacing them with amino acid residues of increasing side chain volume. RyR1-G4934A, -G4941A, and -G4941V mutant channels exhibited a caffeine-induced Ca^{2+} release response in HEK293 cells and bound the RyR-specific ligand [^{3}H]ryanodine. In single channel recordings, significant differences in the number of channel events and mean open and close times were observed between WT and RyR1-G4934A and -G4941A. RyR1-G4934A had reduced K^+ conductance and ion selectivity compared with WT. Mutations further increasing the side chain volume at these positions (G4934V and G4941I) resulted in reduced caffeine-induced Ca^{2+} release in HEK293 cells, low [^{3}H]ryanodine binding levels, and channels that were not regulated by Ca^{2+} and did not conduct Ca^{2+} in single channel measurements. Computational predictions of the thermodynamic impact of mutations on protein stability indicated that although the G4934A mutation was tolerated, the G4934V mutation decreased protein stability by introducing clashes with neighboring amino acid residues. In similar fashion, the G4941A mutation did not introduce clashes, whereas the G4941I mutation resulted in intersubunit clashes among the mutated isoleucines. Co-expression of RyR1-WT with RyR1-G4934V or -G4941I partially restored the WT phenotype, which suggested lessening of amino acid clashes in heterotetrameric channel complexes. The results indicate that both glycines are important for RyR1 channel function by providing flexibility and minimizing amino acid clashes.

The skeletal muscle ryanodine receptor ion channel (RyR1) releases Ca^{2+} from an intracellular membrane compartment, the sarcoplasmic reticulum (SR),[6] to initiate muscle contraction (1). RyR1 is a homotetramer comprised of four 565-kDa RyR1 and four 12-kDa FKPB12 polypeptides (2, 3). The C-terminal portion of the channel complex forms the pore region of RyR1. The large N-terminal domain on the cytoplasmic side is the site of regulation by small cytoplasmic molecules and proteins that include Ca^{2+}, adenine nucleotides, protein kinases, phosphatases and calmodulin, and *in vitro* ligands such as caffeine (4–6). Impaired SR Ca^{2+} release has been linked to mutations in RyR1 associated with muscle diseases malignant hyperthermia and central core disease (2). A majority of the central core disease mutations are in the C-terminal pore-forming region of RyR1 where they form tetrameric channel assemblies that do not conduct Ca^{2+} (7, 8).

Three-dimensional reconstruction of cryo-EMs revealed a 29 × 29 × 12-nm cytoplasmic domain and transmembrane domain measuring 7 nm in length and 8 nm in diameter comprised of six helices (9–15). The pore-forming region consists of an inner S6 helix (~30 residues), a pore helix (~15 residues), and a GGGIG motif similar to the selectivity filter motif T(V/I)GYG of K^+ channels (10, 12–17). In contrast to K^+ channels that selectively conduct K^+ ions, RyRs have a high ion conductance for monovalent (~800 pS with 250 mM K^+ as conducting ion) and divalent cations (~150 pS with 50 mM Ca^{2+}) (18–20). Mutagenesis and single channel measurements showed that conserved RyR luminal RyR1-D4899 and -E4900 and negatively charged amino acid residues lining the cytosolic vestibule are critical for RyR ion permeation and selectivity (21, 22). A tetrameric assembly comprised of the two C-terminal transmembrane segments, the pore helix, and connecting loops conducted K^+ and Ca^{2+} ions but lacked the ability to be gated by Ca^{2+} (23).

In K^+ channels, a bend of the pore-lining helix near a "hinge" glycine has been associated with channel opening (24). The RyR1 S6 pore-lining helix has two glycines, Gly-4934 and Gly-4941 that are conserved in the RyRs. Cryo-EM suggests Gly-4934 and Gly-4941 as possible positions that introduce a bend

* This work was supported, in whole or in part, by National Institutes of Health Grant AR018687.
[1] Present address: Dept. of Biochemistry, School of Basic Medical Sciences, Zhengzhou University, Henan, China.
[2] Present address: Dept. of Epidemiology, University of North Carolina, Chapel Hill, NC 27599.
[3] Present address: Dept. of Medicine, University of Arizona, Tucson, AZ 85724.
[4] These authors contributed equally to this work.
[5] To whom correspondence should be addressed: Dept. of Biochemistry and Biophysics, University of North Carolina, Chapel Hill, NC 27599-7260. Tel.: 919-966-5021; E-mail: meissner@med.unc.edu.

[6] The abbreviation used is: SR, sarcoplasmic reticulum.

in S6 in the open (14) or closed (10, 12, 13, 15) RyR1. Replacement of Gly-4864 in RyR2 (corresponding to Gly-4934 in RyR1) with alanine yielded channels with K^+ conductance and channel open probability comparable with that of WT, which suggested that glycine at position 4934 is not essential for channel gating (25). Substitution of Gly-4864 with Val in RyR2 resulted in the absence of functional channels. In the present study, a combined mutational and computational approach was used to determine how mutations of Gly-4934 and Gly-4941 in S6 pore-lining helix affect RyR1 gating and ion permeation. The results indicate that both glycines are involved in RyR1 channel gating, with RyR1-G4941A altering the kinetics of channel gating to a greater extent than RyR1-G4934A. Increase of the side chain volume at these positions (G4934V and G4941I) resulted in loss of function channels that were not regulated by Ca^{2+} and did not conduct Ca^{2+} in single channel measurements.

Materials and Methods

Preparation of Wild-type and Mutant Channels—Mutations in the full-length rabbit RyR1 were introduced using *pfu* polymerase and mutagenic oligonucleotides following the QuikChange II site-directed mutagenesis kit protocol (Stratagene, La Jolla) (26). WT and mutant RyR1s were expressed in HEK293 cells. Membrane fractions and proteoliposomes that contained recombinant purified WT and mutant RyR1 channels were prepared as described (26).

Ca^{2+} Release Measurements—Cellular Ca^{2+} release was determined as described (21). HEK293 cells grown on glass coverslips were loaded with 5 μM Fluo 4-AM in Krebs-Ringer-Henseleit buffer (125 mM NaCl, 5 mM KCl, 1.2 mM KH_2PO_4, 6 mM glucose, 1.2 mM $MgCl_2$, 2 mM $CaCl_2$, and 25 mM Hepes, pH 7.4). RyR-mediated Ca^{2+} release was induced by the addition of 5 mM caffeine and measured in individual cells using EasyRatioPro (Photon Technology International, Lawrenceville, NJ).

SDS-PAGE and Immunoblot Analyses—Proteins in crude membrane fractions were separated using 3–12% gradient SDS-PAGE. Proteins were transferred overnight to nitrocellulose membranes as described (16), probed with primary rabbit anti-RyR1 polyclonal antibody directed against RyR1 peptide CFIKGLDSFSGKPRGSG and peroxidase-conjugated anti-rabbit IgG (Calbiochem), visualized using enhanced chemiluminescence, and quantified using ImageQuantTL Analysis Software.

[^{3}H]Ryanodine Binding—B_{max} values of [^{3}H]ryanodine binding were determined as described (16). Crude membrane preparations were incubated for 4 h at 24 °C in 20 mM imidazole, pH 7.0, 0.6 M KCl, 0.15 M sucrose, 100 μM Ca^{2+}, protease inhibitors, and nearly saturating concentration of [^{3}H]ryanodine (20 nM) in the absence or presence of 1000-fold excess of unlabeled ryanodine. Unbound [^{3}H]ryanodine was removed using a filter assay. Radioactivity remaining on the filters was determined by liquid scintillation counting to obtain bound [^{3}H]ryanodine.

Single Channel Recordings—Single channel measurements were performed using planar lipid bilayers as described (22). Proteoliposomes that contained purified RyR1s were added to the *cis*, cytosolic chamber of a bilayer apparatus, and recorded in symmetrical 250 mM KCl, 20 mM KHepes, pH 7.4, containing the indicated Ca^{2+} concentrations in the *cis*, cytosolic, and *trans*, SR luminal chambers. A strong dependence of single channel activity on *cis* Ca^{2+} concentration indicated the incorporation of functional channels, with the cytosolic region facing the *cis* chamber of the bilayer. The *trans* side of the bilayer was defined as ground. Electrical signals were filtered at 2 kHz (0.5 kHz for Ca^{2+} currents at 0 mV), digitized at 10 kHz, and analyzed at 50% threshold setting using commercially available software (pClamp, Axon Instruments, CA) (22). To determine permeability ratios, single channel activities were recorded in symmetrical 250 mM KCl solution with 10 mM Ca^{2+} in the *trans* chamber. The permeability ratio of Ca^{2+} *versus* K^+ (P_{Ca}/P_K) was calculated using a modified form of the Goldman-Hodgkin-Katz equation,

$$E_{rev} = -\frac{RT}{F} Ln\left\{[K]^{\frac{1}{2}} \times \left([K] + 4\frac{P_{Ca}}{P_K}[Ca]\right)^{-\frac{1}{2}}\right\} \quad \text{(Eq. 1)}$$

where E_{rev} is the reversal potential, and [K] and [Ca] are the potassium and calcium ion concentrations.

Molecular Modeling of the RyR1 Closed Channel Structure—Amino acid substitutions and rotamer optimizations for the closed 3.8 Å resolution cryo-EM structure (Protein Data Bank code 3J8H) (15) were performed using Eris (27, 28). Structures were subsequently minimized using GROMACS (29) with the GROMOS forcefield (30). Position restraints on backbone atoms for residues within 5 Å of the mutation site were gradually reduced from 1000 to 0 kJ/(mol·nm^2) over 2000 steps of steepest decent minimization. Position restraints on backbone atoms for all other residues remained at 1000 kJ/(mol·nm^2) throughout the minimization.

To prepare the 3.8 Å resolution cryo-EM structure of RyR1 (15) for Eris calculations, the structure was relaxed by performing 100,000 steps of discrete molecular dynamics simulation (31–33) with the Medusa forcefield (34), gradually reducing the temperature from 0.6 (~302 K) to 0.01 (~5 K) kcal/(mol·k_B). All backbone atoms were static throughout the simulation.

Biochemical Assays and Data Analysis—Free Ca^{2+} concentrations were established by adding varying amounts of Ca^{2+} to 1 mM EGTA solutions. Free Ca^{2+} concentrations were determined with the use of a Ca^{2+} selective electrode. Differences between samples were analyzed using Student's *t* test; $p < 0.05$ was considered significant.

Results

Expression and Function of RyR1-G4934 and -G4941 Mutants—RyR1-WT and G4934 and G4941 mutants were expressed in HEK293 cells, and expression levels and function were examined by immunoblot analysis and cellular Ca^{2+} release in response to the Ca^{2+}-releasing drug caffeine, respectively. Retention of function in membrane isolates was probed with a ligand binding assay using [^{3}H]ryanodine. Single channel measurements with purified RyR1s determined the gating and ion permeation properties of WT and mutant channels.

Expression of RyR1-G4934 mutants with Ala and Val substitution and RyR1-G4941 mutants with Ala, Val, and Ile substitution ranged from ~34% (G4941V) to 78% (G4934V) of WT (Fig. 1 and Table 1). A variable caffeine-induced Ca^{2+} release response was observed in 30–50% of HEK293 cells expressing

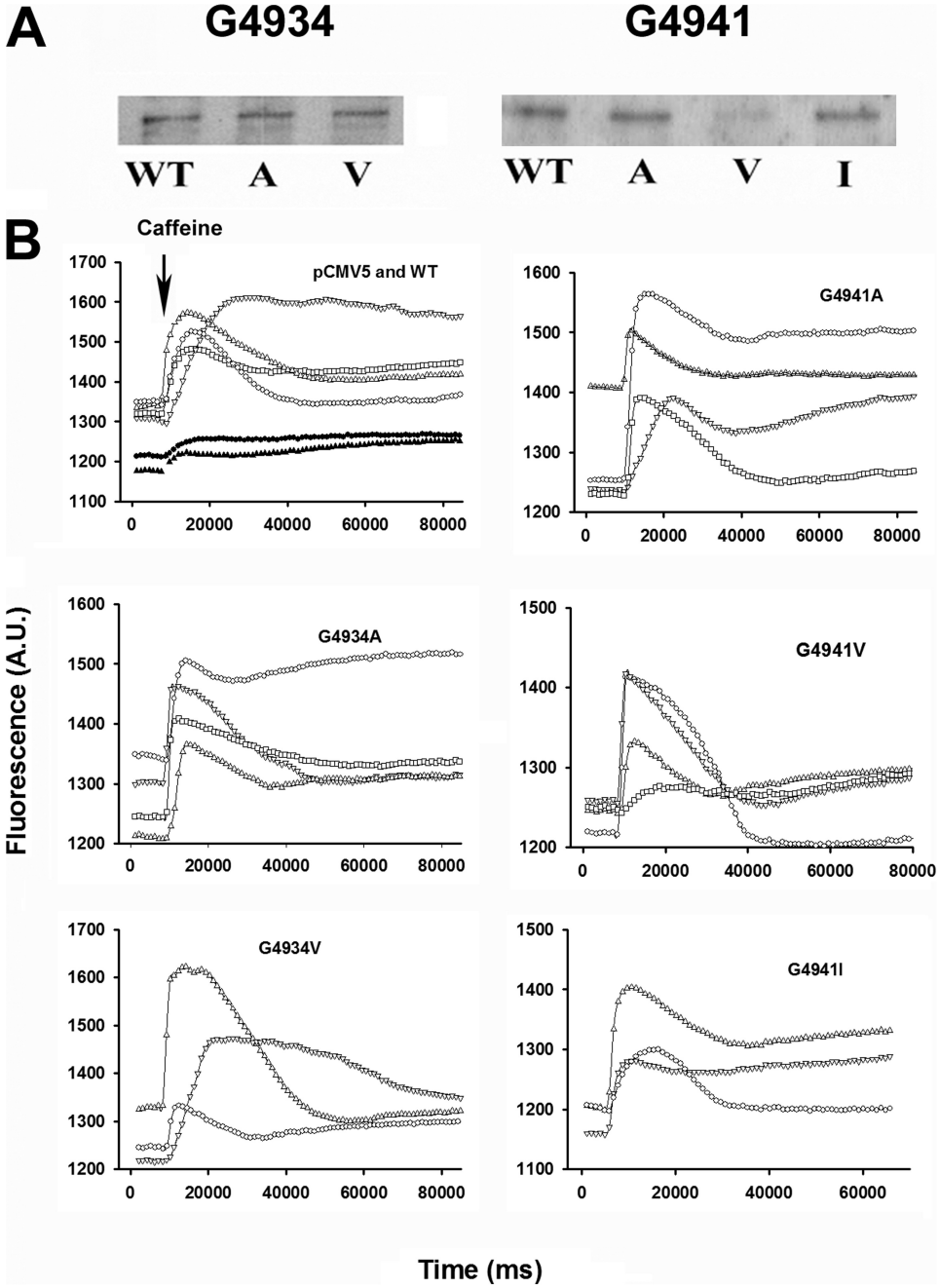

FIGURE 1. **Expression and caffeine-induced Ca^{2+} release of wild-type and mutant RyR1s.** *A*, proteins (20 μg/lane) were separated using 3–12% gradient SDS-PAGE, transferred to nitrocellulose membranes, and probed with primary rabbit anti-RyR1 polyclonal antibody and peroxidase-conjugated rabbit-mouse IgG. *B*, Ca^{2+} transients were determined in Krebs-Ringers Henseleit bath solution as changes of Fluo-4 fluorescence before and following the addition of 5 mM caffeine to the cells (*arrow*). WT, *open symbols*; pCMV5, *closed symbols*. The averaged data are summarized in Table 1.

WT-RyR1. The variable response may have resulted from the nonhomogenous exposure of caffeine to HEK293 cells and removal of released Ca^{2+} by cellular transport systems. Cells expressing RyR1-G4934A and -G4941A had a comparable Ca^{2+} release response, whereas a variable caffeine response in a smaller number of cells expressing RyR1-G4934V, -G4941V, and -G4941I suggested partial loss of Ca^{2+} release function (Fig. 1 and Table 1). A ligand binding assay indicated reduced levels of [^{3}H]ryanodine binding to the mutants compared with WT, with the lowest levels of binding observed for G4934V (14.5% of WT) and G4941I (6.7% of WT) (Table 1).

WT and mutant channels were solubilized using the zwitterionic detergent CHAPS, purified on sucrose gradients, and reconstituted in proteoliposomes that were fused with planar lipid bilayers. Channels were recorded with 250 mM KCl on both sides of the bilayer at *cis*, cytosolic 2 or 0.1 μM Ca^{2+} concentrations that activated or minimally activated WT-RyR1. The addition of 10 mM Ca^{2+} to the *trans*, SR luminal site of the bilayer allowed measurement of Ca^{2+} currents at 0 mV and reversal potentials.

RyR1-WT channels were activated in the presence of 2 μM cytosolic Ca^{2+} (*upper left trace* of Fig. 2*A*). K^+ conductance was

TABLE 1
Properties of WT and mutant channels

	WT	G4934A	G4934V	G4941A	G4941V	G4941I
Immunoblots (% WT)	100	64.3 ± 8.6 (10)[a]	78.0 ± 7.7 (10)	69.5 ± 12.8 (13)[a]	34.4 ± 13.1 (10)[a]	68.9 ± 14.9 (15)[a]
Caffeine response (% WT)	100	99.0 ± 5.9 (6)	17.1 ± 6.8 (6)[a]	86.9 ± 8.8 (10)	69.4 ± 10.8 (9)[a]	31.3 ± 16.3 (3)[a]
B_{max} of [^{3}H]ryanodine binding (% WT)	100	74.5 ± 11.4 (10)[a]	14.5 ± 5.3 (10)[a]	30.7 ± 6.1 (20)[a]	51.1 ± 7.0 (12)[a]	6.7 ± 4.0 (8)[a]
P_o (2 μM Ca^{2+})	0.29 ± 0.04 (19)	0.29 ± 0.06 (19)	0.50 ± 0.13 (12)	0.08 ± 0.03 (12)[a]	0.53 ± 0.04 (13)[a]	0.38 ± 0.11 (12)
P_o (0.1 μM Ca^{2+})	0.01 ± 0.01 (19)	0.01 ± 0.01 (7)	0.52 ± 0.13 (12)	0.01 ± 0.01 (4)	0.01 ± 0.01 (5)	0.22 ± 0.08 (11)
γ_{K^+} (pS)	801 ± 7 (17)	676 ± 5 (25)[a]	564 ± 63 (12)	771 ± 7 (12)	799 ± 3 (13)	585 ± 98 (12)
I_{ca} (+10 mM trans Ca^{2+}) (pA)	−2.5 ± 0.1 (12)	−1.6 ± 0.1 (7)[a]	0.1 ± 0.1 (12)	2.3 ± 0.1 (8)	−2.8 ± 0.1 (7)	0.1 ± 0.1 (10)
P_{Ca}/P_K	6.7 ± 0.2 (12)	5.4 ± 0.3 (6)[a]	ND[b]	6.6 ± 0.3 (8)	6.9 ± 0.2 (6)	ND
No. of events/min (2 μM Ca^{2+})	23,821 ± 2001 (19)	13,924 ± 1743 (19)[a]	ND	3605 ± 800 (10)[a]	6400 ± 818 (13)[a]	ND
τ_o (ms) (2 μM Ca^{2+})	0.68 ± 0.06 (19)	0.92 ± 0.10 (19)	ND	1.23 ± 0.21 (10)[a]	4.98 ± 0.72 (13)[a]	ND
τ_c (ms) (2 μM Ca^{2+})	2.39 ± 0.37 (19)	4.28 ± 0.81 (19)[a]	ND	19.4 ± 3.4 (10)[a]	3.94 ± 0.27 (13)[a]	ND

[a] $p < 0.05$ compared with WT.
[b] ND, not determined.

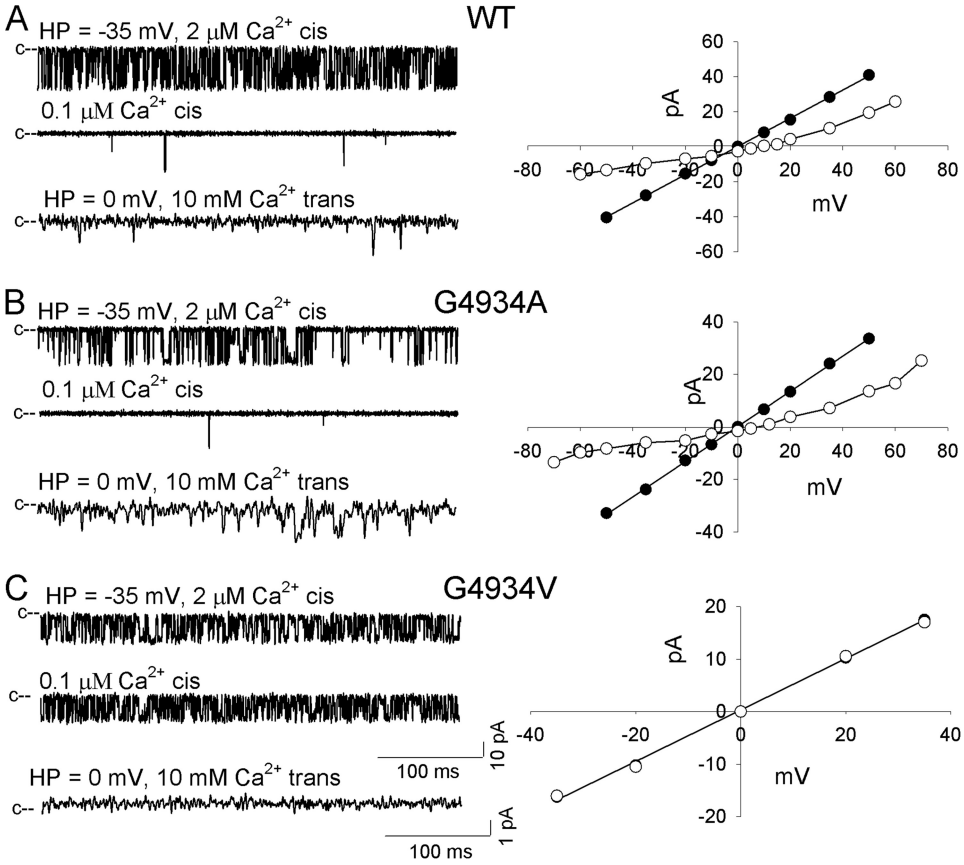

FIGURE 2. **Single channel measurements of RyR1-WT and -G4934 mutant channels.** *Left panels*, representative single channel currents at −35 mV (*upper* and *second traces* of *A–C*) or 0 mV (*bottom traces* of *A–C*) shown as downward deflections from the closed states (*c*−) in symmetrical 250 mM KCl with 2 μM Ca^{2+} in the *cis* chamber (*upper traces* of *A–C*) and after the subsequent addition of EGTA to yield free Ca^{2+} of 0.1 μM (*second traces* of *A–C*) or addition of 10 mM Ca^{2+} to the trans chamber (*bottom traces* of *A–C*). *Right panels*, representative current voltage relationships in 250 mM symmetrical KCl (●) and after addition of 10 mM trans Ca^{2+} (○). Current and time scales for single channel traces are as shown. Averaged P_o values and ion permeation properties are summarized in Table 1.

801 ± 7 pS (Fig. 2*A*, *right panel*, and Table 1). Reduction of cytosolic Ca^{2+} to 0.1 μM reduced channel open probability (P_o) to nearly 0 (Fig. 2*A*, *second trace* on *left*, and Table 1). In the presence of 10 mM SR luminal Ca^{2+}, a Ca^{2+} current of −2.5 pA at 0 mV was obtained (Fig. 2*A*, *third trace* and *right panel*, and Table 1). Applying constant field theory, reversal potential (E_{rev}) of 9.2 mV yielded a permeability ratio of Ca^{2+} over K^+ (P_{Ca}/P_K) of 6.7 for WT (Table 1).

Mutations of RyR1-G4934 or -G4941 resulted in functional (G4934A, G4941A, and G4941V) and loss of function (G4934V and G4941I) channels (Figs. 2 and 3). Functional channels were gated by Ca^{2+} similar to WT, having a significantly higher P_o at 2 μM cytosolic Ca^{2+} compared with 0.1 μM Ca^{2+} (Table 1). However, significant differences were observed between WT and functional mutant channels with regard to P_o, number of channel events, and mean open and close times. RyR1-G4934A and WT had the same mean P_o (0.29), whereas RyR1-G4941A had a reduced (0.08 *versus* 0.29) and G4941V an elevated (0.53 *versus* 0.29) P_o compared with WT. Kinetic analysis showed a significant decrease in the number of channel events between WT (23,821/min), RyR1-G4934A (13,924/min), RyR1-G4941A (3605/min), and RyR1-G4941V (6400/min). RyR1-G4941A and -G4941V had increased open times (1.23 and 4.98 ms *versus* 0.68 ms for WT). All three mutants exhibited increased mean

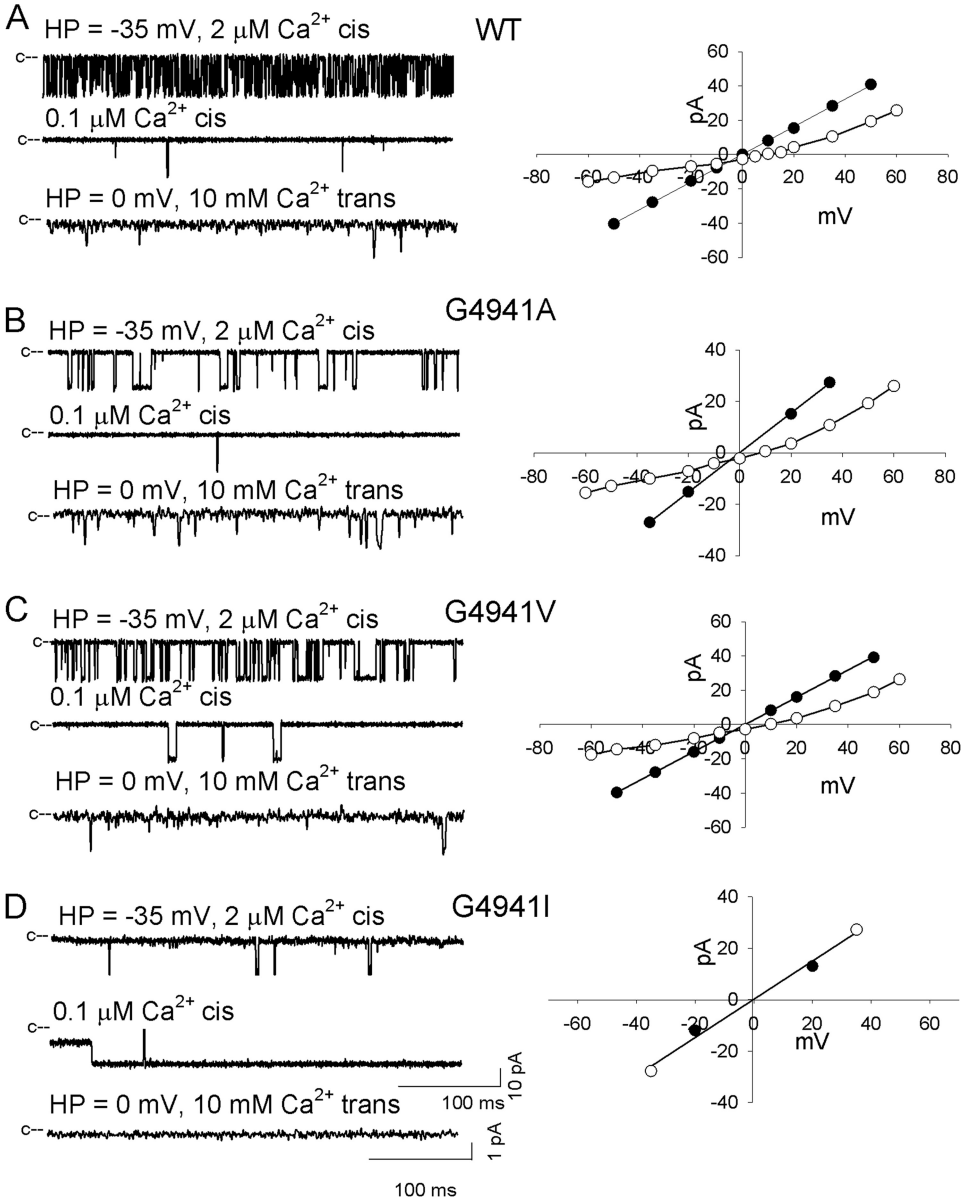

FIGURE 3. **Single channel measurements of RyR1-WT and -G4941 mutant channels.** *Left panels*, representative single channel currents at −35 mV (*upper* and *second traces* of *A–D*) or 0 mV (*bottom traces* of *A–D*) shown as downward deflections from the closed states (*c*−) in symmetrical 250 mM KCl with 2 μM Ca^{2+} in the *cis* chamber (*upper traces* of *A–D*) and after the subsequent addition of EGTA to yield free Ca^{2+} of 0.1 μM (*second traces* of *A–D*) or addition of 10 mM Ca^{2+} to the trans chamber (*bottom traces of A–D*). *Right panels*, representative current voltage relationships in 250 mM symmetrical KCl (●) and after the addition of 10 mM trans Ca^{2+} (○). Current and time scales for single channel traces are as shown. Averaged P_o values and ion permeation properties are summarized in Table 1.

close times (4.28 ms for G4934A, 19.4 ms for G4941A, and 3.94 ms for G4941V *versus* 2.39 ms for WT). Single channel K^+ conductance was significantly reduced for RyR1-G4934A (676 pS *versus* 801 pS for WT). In the presence of 10 mM trans, luminal Ca^{2+}, a reduced Ca^{2+} current ($I_{Ca} = -1.6$ *versus* −2.5 pA for WT) was measured. Applying constant field theory, a decreased reversal potential ($E_{rev} = 7.8$ mV *versus* 9.2 mV for WT) yielded a permeability ratio of Ca^{2+} over K^+ (P_{Ca}/P_K) of 5.4 for RyR1-G4934A compared with 6.7 for WT. K^+ conductances and permeability ratios of RyR1-G4941A and -G4941V were not altered by the mutations.

Loss of function channels (G4934V and G4941I) exhibited variable K^+ conductances, absence of Ca^{2+} currents at 0 mV, and P_o values that were not substantially reduced by lowering cytosolic Ca^{2+} from 2 to 0.1 μM (Table 1). Taken together, data of Figs. 2 and 3 and Table 1 indicate that substitution of Gly-4934 with Ala and Gly-4941 with Ala and Val resulted in functional channels with altered single channel properties, whereas replacement of Gly-4934 with Val and Gly-4941 with Ile resulted in channels with abnormal channel behavior in lipid bilayer measurements.

Heterotetrameric RyR1-WT and -G4934V Ion Channels—Simultaneous expression of WT and mutant channels in HEK293 resulted in heterotetrameric channels that differed in their gating and ion permeation properties (8, 35, 36). Whether Ca^{2+}-dependent channel activity and Ca^{2+} currents were restored in RyR1-G4934V by forming heterotetrameric channels composed of WT and G4934V was addressed by co-trans-

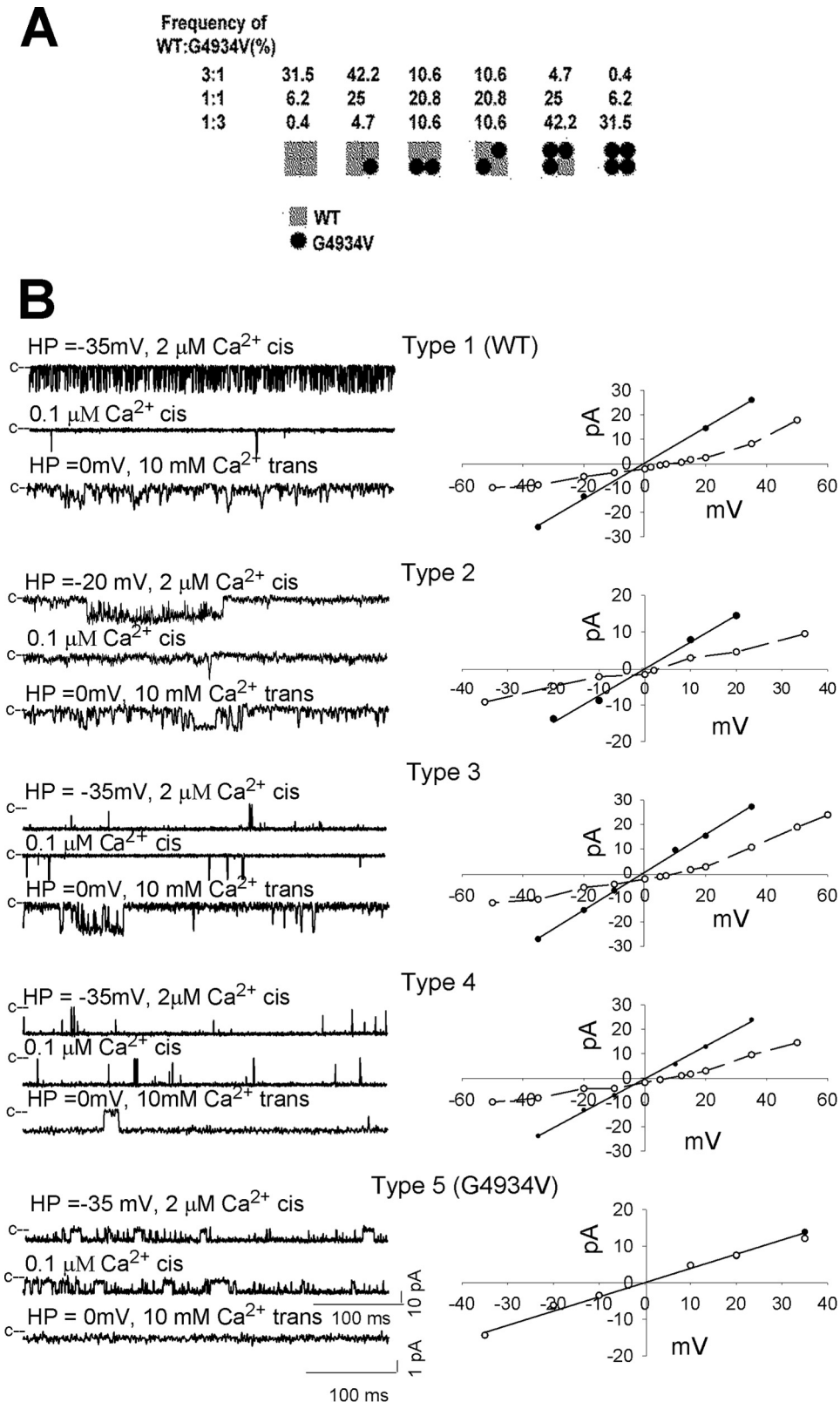

FIGURE 4. **Single channel measurements of homotetrameric and heterotetrameric RyR1-WT and -G4934V channel complexes.** *A*, subunit distribution and frequency of channel complexes in cells expressing WT and mutant subunits at indicated ratios, assuming uniform distribution of subunits. *B*, representative single channel measurements were performed and analyzed as in Fig. 2. Current and time scales for single channel traces are as shown. Averaged P_o values and ion permeation properties are summarized in Table 2.

TABLE 2
Single channel properties of purified heterotetrameric WT and G4934V RyR1s

	P_o				
	2 μM Ca	0.1 μM Ca	γ_K^+	I_{Ca} (+10 mM Ca trans)	P_{Ca}/P_K
			pS	*pA*	
Type 1 (WT)	0.30 ± 0.07 (10)	0.02 ± 0.02 (10)	764 ± 9 (10)	−2.2 ± 0.1 (10)	6.7 ± 0.1 (10)
Type 2	0.31 ± 0.13 (3)	0.07 ± 0.04 (3)	740 ± 31 (3)	−1.5 ± 0.1 (3)[a]	1.7 ± 0.3 (3)[a]
Type 3	0.91 ± 0.03 (6)[a]	0.12 ± 0.06 (6)	772 ± 9 (6)	−2.3 ± 0.1 (6)	7.1 ± 0.1 (6)[a]
Type 4	0.96 ± 0.02 (13)[a]	0.90 ± 0.05 (13)[a]	691 ± 11 (13)[a]	−1.8 ± 0.1 (13)[a]	6.1 ± 0.4 (13)
Type 5 (G4934V)	0.59 ± 0.07 (40)[a]	0.59 ± 0.06 (40)[a]	598 ± 55 (40)	0.1 ± 0.1 (40)[a]	ND[b]

[a] $p < 0.05$ compared to WT.
[b] ND, not determined.

TABLE 3
Number of channel types determined from single channel measurements

Number of experimentally determined WT, heterotetrameric, and homotetrameric mutant (mutant) channels at indicated expression vector ratios using 7 μg of total DNA/dish. In parentheses is the number of channels assuming uniform distribution of subunits in the channel complexes and WT and mutant subunits at immunoblot ratios shown in Table I.

RyR1 expression vector ratio	RyR1 channel types		
	WT	Heterotetrameric	Mutant
WT:G4934V			
3:1	9 (10.7)	6 (16.3)	12 (0.03)
1:1	0 (1.8)	5 (15.5)	13 (0.7)
1:3	1 (0.2)	11 (20.3)	15 (6.5)
WT:G4941I			
3:1	8 (11.3)	10 (14.6)	8 (0.03)
1:1	9 (2.7)	4 (18.7)	9 (0.5)
1:3	4 (0.2)	0 (15.6)	16 (4.2)

fecting HEK293 cells with RyR1-WT and RyR1-G4934V expression vectors at ratios of 3:1, 1:1, and 1:3. Assuming uniform distribution of WT and mutant subunits, six channel types could be potentially formed (Fig. 4*A*). Channels comprised of four and three WT subunits were expected to predominate in cells expressing RyR1-WT and RyR1-G4934V at 3:1 ratio. Conversely, channels with four or three mutant subunits were favored in cells expressing WT and mutants at 1:3 ratio. We observed five channel types that differed in their gating and ion permeation characteristics in 72 single channel measurements (Fig. 4*B* and Table 2). Channel types 1 and 5 exhibited single channel properties that suggested homotetrameric channels corresponding to RyR1-WT and RyR1-G4934V, respectively. Type 2 channels exhibited cytosolic Ca^{2+} single channel open probabilities comparable with WT in the presence of 2 and 0.1 μM *cis*, but with a reduced Ca^{2+} current and Ca^{2+} selectivity compared with WT. Type 3 and 4 channels had P_o values close to 1 at 2 μM Ca^{2+} with type 3 having low P_o at 0.1 μM cytosolic Ca^{2+}. Type 4 channels maintained $P_o \sim 1$ at 0.1 μM cytosolic Ca^{2+}. A second distinguishing feature was that type 3 channels had increased Ca^{2+} selectivity, whereas type 4 channels displayed a significantly reduced K^+ conductance and Ca^{2+} current compared with WT. Table 3 compares the number of experimentally determined and calculated channel types assuming uniform distribution of wild-type and mutant subunits expressed in HEK293 cells at ratios shown in Table 1. Type 1 (WT) channels were mostly found, as expected, in HEK293 cells with WT:G4934V = 3:1 (9 of 27 recordings). Type 5 (G4934V) channels were identified in preparations isolated from cells with WT:G4941V ratio of 3:1 (12 of 27 recordings), 1:1 (13 of 18), and 1:3 (15 of 27). We ascribe the large number of loss of function channels to the instability of channels comprised of one, two, and possibly three mutant subunits. We observed no clear preference for type 2, 3, and 4 channels in cells with WT:G4941V ratios of 3:1, 1:1, and 1:3.

Heterotetrameric WT and G4941I Ion Channels—RyR1-WT and RyR1-G4941I were also expressed at ratios of 3:1, 1:1, and 1:3. Sixty-eight single channel measurements indicated the presence of six channel types that differed in their gating and ion permeation characteristics (Fig. 5 and Table 4). This suggested that channels with zero (WT), one, two, and three (heterotetrameric channels) and four (G4941I) mutant subunits were recorded. Types 1 and 6 exhibited properties that suggested recording of homotetrameric channels corresponding to RyR1-WT and RyR1-G4941I, respectively. Type 2 channels exhibited single channel open probabilities comparable with WT in the presence of 2 and 0.1 μM *cis*, cytosolic Ca^{2+} but had reduced Ca^{2+} current and Ca^{2+} selectivity compared with WT. Type 3, 4, and 5 channels had P_o values close to 1 at 2 μM Ca^{2+}. However, type 3 had low P_o values at 0.1 μM cytosolic Ca^{2+}, whereas types 4 and 5 maintained P_o values close to 1 at 0.1 μM cytosolic Ca^{2+} with type 4 channels displaying P_{Ca}/P_K comparable with WT and with type 5 channels having significantly reduced Ca^{2+} current and Ca^{2+} selectivity compared with WT. Type 1 (WT) channels were mostly found in HEK293 cells with WT:G4934V = 3:1 and 1:1 (8 of 26 and 9 of 22 recordings, respectively) (Table 3). Type 6 (G4941I) channels were recorded in preparations isolated from cells with WT:G4941I ratio of 3:1 (8 of 26 recordings), 1:1 (9 of 22 recordings), and 1:3 (16 of 20 recordings). A majority of heterotetrameric channels came from cells with WT: G4941V ratio of 3:1 (10 of 26 recordings). Four type 2–5 channels were identified in cells with ratio of 1:1 and no type 2–5 channels from cells with ratio of 1:3. Table 3 shows that the number of measured homotetrameric mutant channels was greater than the calculated number of channels. This suggested instability of channels comprised of WT and mutant subunits.

Discussion

Glycine residues often confer flexibility to protein structures, making RyR1-G4934 and -G4941 good candidates as movable hinges during channel opening and closing. This study therefore investigated the role of the two glycines in the pore-lining S6 helix in RyR1 channel gating and ion permeation. RyR1-G4934A, -G4941A, and -G4941V formed channels that responded to caffeine in HEK293 cells, bound [^{3}H]ryanodine, and were regulated by Ca^{2+} in single channel measurements. G4934A but not G4941A and G4941V had reduced K^+ conductance and Ca^{2+} selectivity compared with WT. Analysis of

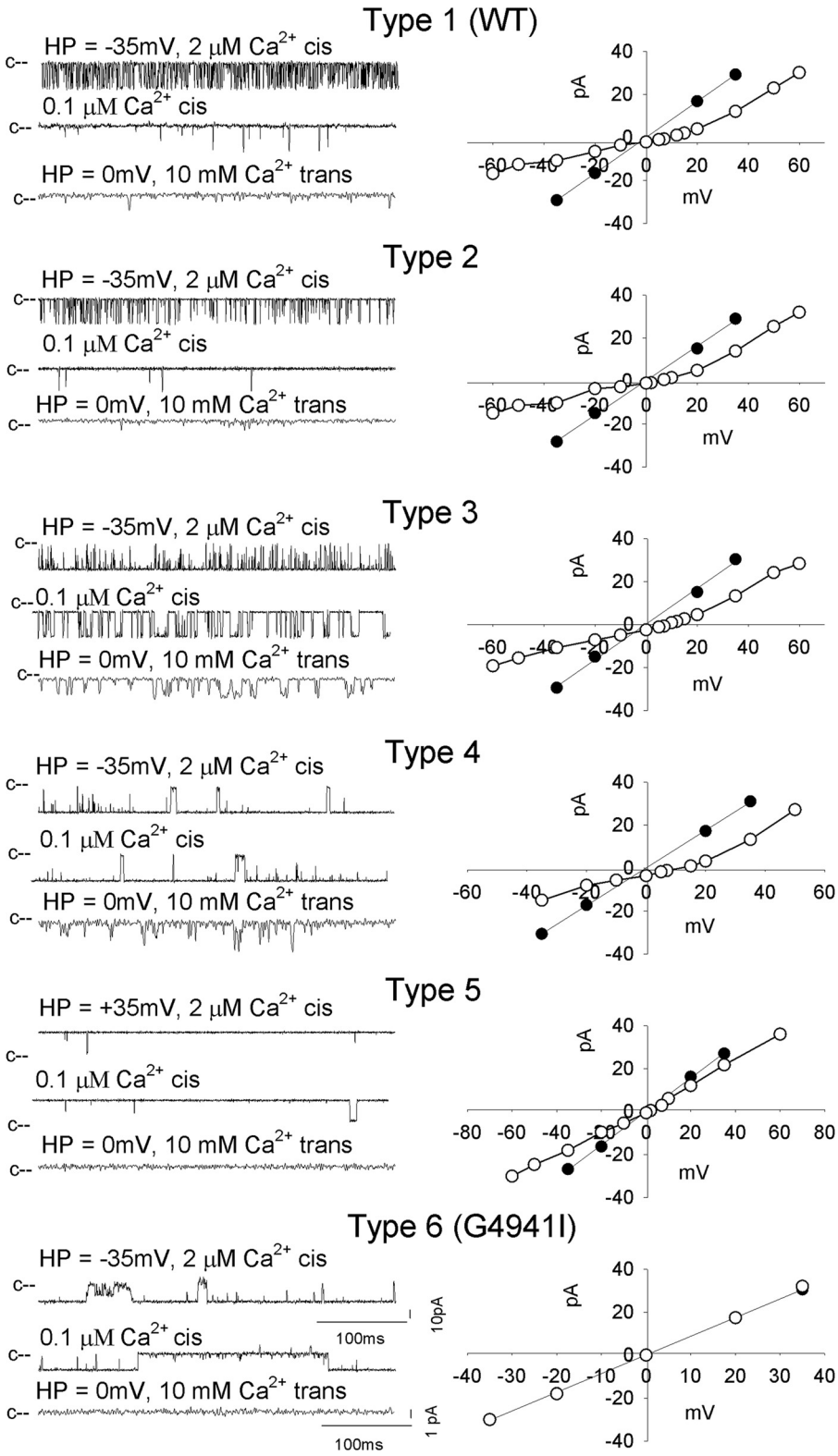

FIGURE 5. **Single channel measurements of homotetrameric and heterotetrameric RyR1-WT and -G4941I channel complexes.** Representative single channel measurements were performed and analyzed as in Fig. 2. Current and time scales for single channel traces are as shown. Averaged P_o values and ion permeation properties are summarized in Table 4.

single channel recordings of mutants with glycine to alanine substitution indicated greater involvement of RyR1-G4941 than RyR1-G4934 in channel gating. Replacement of Gly-4934 with Val and Gly-4941 with Ile resulted in channels with greatly reduced caffeine-induced Ca^{2+} release, low levels of [^{3}H]ryanodine binding, and channels that did not conduct Ca^{2+} or respond to a change in cytosolic Ca^{2+}. The results suggested that increased side chain volume in RyR1-G4934V and -G4941I

TABLE 4
Single channel properties of purified heterotetrameric wild-type and G4941I RyR1s

	P_o				
	2 μM Ca	0.1 μM Ca	γ_K^+	I_0 (+10 mM Ca trans)	P_{Ca}/P_K
			pS	*pA*	
Type 1 (WT)	0.20 ± 0.04 (21)	0.01 ± 0.01 (21)	817 ± 6 (21)	−2.2 ± 0.1 (21)	6.3 ± 0.1 (21)
Type 2	0.16 ± 0.05 (7)	0.04 ± 0.04 (7)	762 ± 38 (7)	−1.4 ± 0.1 (7)[a]	1.7 ± 0.3 (7)[a]
Type 3	0.88 ± 0.05 (3)[a]	0.17 ± 0.05 (3)[a]	835 ± 6 (3)	−2.6 ± 0.1 (3)	6.5 ± 0.1 (3)
Type 4	0.90 (2)	0.95 (2)	880 (2)	−3.2 (2)	7.0 (2)
Type 5	0.99 (2)	0.99 (2)	779 (2)	−0.5 (2)	0.6 (2)
Type 6 (G4941I)	0.53 ± 0.07 (33)[a]	0.52 ± 0.07 (33)[a]	641 ± 59 (33)	0.1 ± 0.1 (33)	ND[b]

[a] $p < 0.05$ compared to WT.
[b] ND, not determined.

introduced structural changes in RyR1 resulting in abnormal behavior in single channel measurements.

There has been precedence suggesting the importance of glycine residues in regulating protein structure and function. In K^+ channels, a bend in the pore-lining S6 helix at a glycine was associated with channel opening (24). Introduction of alanine in Shaker's S6 segment (which stabilizes α-helices) resulted in loss of function channels (37–39). On the other hand, mutagenesis indicated that two S6 glycine residues in hERG were not required for channel function (40). In RyR2, replacement of Gly-4864 in the pore-lining S6 helix (corresponding to Gly-4934 in RyR1) with alanine did not markedly alter the caffeine response in HEK293 cells or the interaction with ryanodine or resulted in significant differences in K^+ conductance and channel open probability at different cytosolic Ca^{2+} concentrations (25, 41). At variance, we observed that replacement of Gly-4934 in RyR1 with Ala significantly reduced single channel K^+ conductance and ion selectivity for Ca^{2+} compared with K^+. The amino acid sequences of the inner S6 helix of RyR1 and RyR2 are highly homologous; however, it is possible that structural differences in other regions account for the differences in the channel properties of the RyR2-G4864A and RyR1-G4934A mutants. Single channel measurements after replacing amino residues with increased side chain volume demonstrated the importance of RyR1-G4941 in a proposed hinge region of the RyR1 pore.

We used the 3.8 Å resolution structure of the closed channel RyR1 (Protein Data Bank code 3J8H) as structural template (15) for modeling our mutant data. Although there are open structural models of RyR1, they are as yet of insufficient resolution to serve as a basis for our modeling (14, 16). We propose that in the closed channel, RyR1-G4934A increases intersubunit interactions between residue position 4934 and residues on the adjacent S6 helix (Ile-4936, Ile-4937, and Phe-4940) (Fig. 6, *A* and *B*), potentially explaining the moderate functional effects of the G4934A mutation observed in the single channel experiments. Stabilization of the S6 helix by alanine may have contributed to functional changes of RyR1-G4934A. When RyR1-G4934 is mutated to valine, the contacts with the neighboring amino acid residues become more extensive, potentially explaining the reduced function observed with the RyR1-G4934V mutant in the cellular and ligand binding experiments and the lack of function in single channel measurements.

The G4941A mutation altered channel closed times to a greater extent than the G4934A mutation, with the G4941V mutation restoring channel closed times more similar to

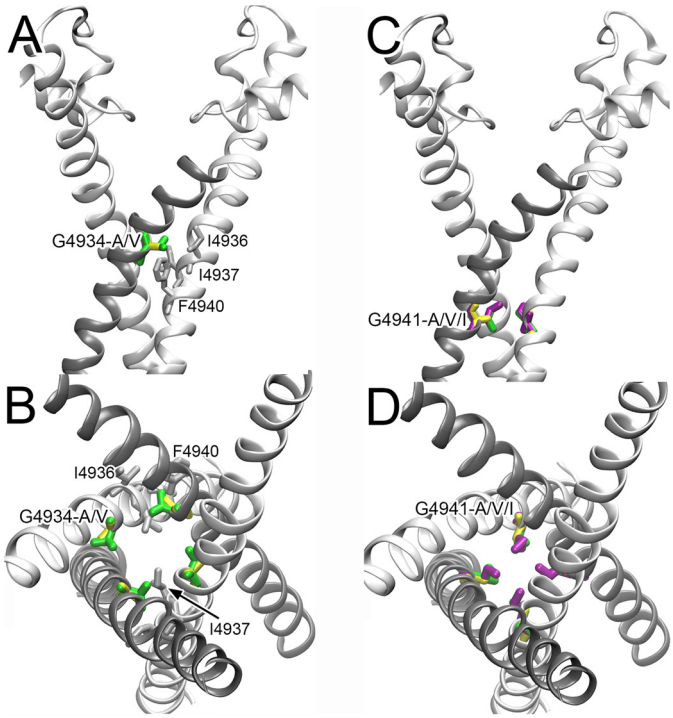

FIGURE 6. **RyR1-G4934 (*A* and *B*) and RyR1-G4941 (*C* and *D*) mutations depicted in the RyR1 closed channel structure.** Ala, Val, and Ile substitutions are shown in *yellow*, *green*, and *purple*, respectively. *A* and *B*, side (*A*) and luminal (*B*) views of the 3.8 Å resolution RyR1 closed channel structure (15) show that mutations of RyR1-G4934 to Ala and Val increase contacts with Ile-4936, Ile-4937, and Phe-4940 of the neighboring subunit. The G4934V mutation produces particularly close contacts with Ile-4937, which may result in structural perturbation yielding loss-of-function channels. *C* and *D*, side (*C*) and luminal (*D*) views of the RyR1 closed channel structure show that Ala, Val, and Ile substitutions at RyR1-G4941 result in side chains that progressively protrude into the pore. RyR1-G4941I mutation results in steric hindrances that may cause structural distortion and result in loss of function channels in [^{3}H]ryanodine binding and lipid bilayer measurements.

G4934A and WT. The 3.8 Å resolution structure of the closed channel (15) suggests that the G4941I mutation results in steric clashes (Fig. 6, *C* and *D*) that result in loss of function channels. Because the RyR1-G4941V mutant functions more like WT RyR1 and Val is larger than Ala, it follows that, unlike the 4934 position, the alanine mutation effects at the 4941 position were not brought about by side chain volume. In this case, mutation of the glycine residue likely functions more to affect dynamics of channel gating than imposing steric hindrances. Amino acids with branching at the β carbon, as is the case with valine, can significantly destabilize α helices in comparison to alanine (42). The results suggest that conformational changes at the RyR1 4941 amino acid position change channel gating.

Whether formation of heterotetrameric channels containing WT and RyR1-G4934V or -G4941I subunits would result in partial restoration of channel function was addressed by expressing in HEK293 cells WT and mutant RyR1s at varying ratios. Single channel measurements indicated up to six channel types. In addition to single channel behavior equivalent to homozygous WT and RyR1-G4934V or -G4941I mutant channels, channel types represented by heterotetrameric channels were observed that differed in gating and ion permeation properties. Three heterotetrameric channel types were seen with the co-expression of WT and RyR1-G4934V, and four heterotetrameric channel types were seen with co-expression of WT and RyR1-G4941I at varying ratios. Although there seemed to have been a disproportionate instability of channels having mutant subunits, the experimentally observed occurrence of three heterotetrameric WT:G4934V channel types suggested channels with 1 and 2 and possibly three mutant subunits that partially restored the WT phenotype by responding to Ca^{2+} and conducting Ca^{2+} to varying extents. For WT:G4941I, presence of six channel types suggested partial restoration of the WT phenotype in heterotetrameric channel complexes comprised of one, two, and three RyR1-G4941I subunits.

In conclusion, our studies showed that mutagenesis of two glycine residues in the pore-lining helix of RyR1 altered channel gating and ion conductance. Alanine substitutions likely increased intersubunit interactions and stabilized the pore-lining helix, whereas replacement of RyR1-G4934 with Val and RyR1-G4941 with Ile suggested steric clashes between amino acid residues of the pore-lining helices. The results suggest that two glycines in pore-lining S6 helix facilitate RyR1 channel gating.

References

1. Franzini-Armstrong, C., and Protasi, F. (1997) Ryanodine receptors of striated muscles: a complex channel capable of multiple interactions. *Physiol. Rev.* **77,** 699–729
2. Lanner, J. T. (2012) Ryanodine receptor physiology and its role in disease. *Adv. Exp. Med. Biol.* **740,** 217–234
3. Hamilton, S. L., and Serysheva, I. I. (2009) Ryanodine receptor structure: progress and challenges. *J. Biol. Chem.* **284,** 4047–4051
4. Fill, M., and Copello, J. A. (2002) Ryanodine receptor calcium release channels. *Physiol. Rev.* **82,** 893–922
5. Meissner, G. (2002) Regulation of mammalian ryanodine receptors. *Front. Biosci.* **7,** d2072–d2080
6. Wehrens, X. H., Lehnart, S. E., and Marks, A. R. (2005) Intracellular calcium release and cardiac disease. *Annu. Rev. Physiol.* **67,** 69–98
7. Dirksen, R. T., and Avila, G. (2002) Altered ryanodine receptor function in central core disease: leaky or uncoupled Ca^{2+} release channels? *Trends Cardiovasc. Med.* **12,** 189–197
8. Xu, L., Wang, Y., Yamaguchi, N., Pasek, D. A., and Meissner, G. (2008) Single channel properties of heterotetrameric mutant RyR1 ion channels linked to core myopathies. *J. Biol. Chem.* **283,** 6321–6329
9. Radermacher, M., Rao, V., Grassucci, R., Frank, J., Timerman, A. P., Fleischer, S., and Wagenknecht, T. (1994) Cryo-electron microscopy and three-dimensional reconstruction of the calcium release channel/ryanodine receptor from skeletal muscle. *J. Cell Biol.* **127,** 411–423
10. Ludtke, S. J., Serysheva, I. I., Hamilton, S. L., and Chiu, W. (2005) The pore structure of the closed RyR1 channel. *Structure* **13,** 1203–1211
11. Serysheva, I. I., Orlova, E. V., Chiu, W., Sherman, M. B., Hamilton, S. L., and van Heel, M. (1995) Electron cryomicroscopy and angular reconstruction used to visualize the skeletal muscle calcium release channel. *Nat. Struct. Biol.* **2,** 18–24
12. Efremov, R. G., Leitner, A., Aebersold, R., and Raunser, S. (2015) Architecture and conformational switch mechanism of the ryanodine receptor. *Nature* **517,** 39–43
13. Zalk, R., Clarke, O. B., des Georges, A., Grassucci, R. A., Reiken, S., Mancia, F., Hendrickson, W. A., Frank, J., and Marks, A. (2015) Structure of a mammalian ryanodine. *Nature* **517,** 44–49
14. Samsó, M., Feng, W., Pessah, I. N., and Allen, P. D. (2009) Coordinated movement of cytoplasmic and transmembrane domains of RyR1 upon gating. *PLoS Biol.* **7,** e85
15. Yan, Z., Bai, X. C., Yan, C., Wu, J., Li, Z., Xie, T., Peng, W., Yin, C. C., Li, X., Scheres, S. H., Shi, Y., and Yan, N. (2015) Structure of the rabbit ryanodine receptor RyR1 at near-atomic resolution. *Nature* **517,** 50–55
16. Ramachandran, S., Chakraborty, A., Xu, L., Mei, Y., Samsó, M., Dokholyan, N. V., and Meissner, G. (2013) Structural determinants of skeletal muscle ryanodine receptor gating. *J. Biol. Chem.* **288,** 6154–6165
17. Gao, L., Balshaw, D., Xu, L., Tripathy, A., Xin, C., and Meissner, G. (2000) Evidence for a role of the lumenal M3-M4 loop in skeletal muscle Ca^{2+} release channel (ryanodine receptor) activity and conductance. *Biophys. J.* **79,** 828–840
18. Liu, Q. Y., Lai, F. A., Rousseau, E., Jones, R. V., and Meissner, G. (1989) Multiple conductance states of the purified calcium release channel complex from skeletal sarcoplasmic reticulum. *Biophys. J.* **55,** 415–424
19. Smith, J. S., Imagawa, T., Ma, J., Fill, M., Campbell, K. P., and Coronado, R. (1988) Purified ryanodine receptor from rabbit skeletal muscle is the calcium-release channel of sarcoplasmic reticulum. *J. Gen. Physiol.* **92,** 1–26
20. Tinker, A., and Williams, A. J. (1992) Divalent cation conduction in the ryanodine receptor channel of sheep cardiac muscle sarcoplasmic reticulum. *J. Gen. Physiol.* **100,** 479–493
21. Wang, Y., Xu, L., Pasek, D. A., Gillespie, D., and Meissner, G. (2005) Probing the role of negatively charged amino acid residues in ion permeation of skeletal muscle ryanodine receptor. *Biophys. J.* **89,** 256–265
22. Xu, L., Wang, Y., Gillespie, D., and Meissner, G. (2006) Two rings of negative charges in the cytosolic vestibule of type-1 ryanodine receptor modulate ion fluxes. *Biophys. J.* **90,** 443–453
23. Euden, J., Mason, S. A., and Williams, A. J. (2013) Functional characterization of the cardiac ryanodine receptor pore-forming region. *PLoS One* **8,** e66542
24. Jiang, Y., Lee, A., Chen, J., Cadene, M., Chait, B. T., and MacKinnon, R. (2002) The open pore conformation of potassium channels. *Nature* **417,** 523–526
25. Euden, J., Mason, S. A., Viero, C., Thomas, N. L., and Williams, A. J. (2013) Investigations of the contribution of a putative glycine hinge to ryanodine receptor channel gating. *J. Biol. Chem.* **288,** 16671–16679
26. Gao, L., Tripathy, A., Lu, X., and Meissner, G. (1997) Evidence for a role of C-terminal amino acid residues in skeletal muscle Ca^{2+} release channel (ryanodine receptor) function. *FEBS Lett.* **412,** 223–226
27. Yin, S., Ding, F., and Dokholyan, N. V. (2007) Eris: an automated estimator of protein stability. *Nat. Methods* **4,** 466–467
28. Yin, S., Ding, F., and Dokholyan, N. V. (2007) Modeling backbone flexibility improves protein stability estimation. *Structure* **15,** 1567–1576
29. Hess, B., Kutzner, C., van der Spoel, D., and Lindahl, E. (2008) GROMACS 4: Algorithms for highly efficient, load-balanced and scalable molecular simulation. *J. Chem. Theory Comput.* **4,** 435–447
30. Oostenbrink, C., Villa, A., Mark, A. E., and van Gunsteren, W. F. (2004) A bimolecular force field based on free enthalpy of hydration and solvation: the GROMACS force-field parameter sets 53A5 and 53A6. *J. Comput. Chem.* **25,** 1656–1676
31. Ding, F., Tsao, D., Nie, H., and Dokholyan, N. V. (2008) *Ab infinito* folding of proteins with all-atom discrete molecular dynamics. *Structure* **16,** 1010–1018
32. Dokholyan, N. V., Buldyrev, S. V., Stanley, H. E., and Shakhnovich, E. I. (1998) Discrete molecular dynamics studies of the folding of a protein-like model. *Fold Des.* **3,** 577–587
33. Shirvanyants, D., Ding, F., Tsao, D., Ramachandran, S., and Dokholyan, N. V. (2012) Discrete molecular dynamics: an efficient and versatile simulation method for fine protein characterization. *J. Phys. Chem. B* **116,** 8375–8382

34. Ding, F., and Dokholyan, N. V. (2006) Emergence of protein fold families through rational design. *PLoS Comput. Biol.* **2,** e85
35. Zhao, M., Li, P., Li, X., Zhang, L., Winkfein, R. J., and Chen, S. R. (1999) Molecular identification of the ryanodine receptor pore-forming segment. *J. Biol. Chem.* **274,** 25971–25974
36. Xiao, B., Masumiya, H., Jiang, D., Wang, R., Sei, Y., Zhang, L., Murayama, T., Ogawa, Y., Lai, F. A., Wagenknecht, T., and Chen, S. R. (2002) Isoform-dependent formation of heteromeric Ca^{2+} release channels (ryanodine receptors). *J. Biol. Chem.* **277,** 41778–41785
37. Rosenhouse-Dantsker, A., and Logothetis, D. E. (2006) New roles for a key glycine and its neighboring residue in potassium channel gating. *Biophys. J.* **91,** 2860–2873
38. Magidovich, E., and Yifrach, O. (2004) Conserved gating hinge in ligand- and voltage-dependent K^+ channels. *Biochemistry* **43,** 13242–13247
39. Ding, S., Ingleby, L., Ahern, C. A., and Horn, R. (2005) Investigating the putative glycine hinge in Shaker potassium channel. *J. Gen. Physiol.* **126,** 213–226
40. Hardman, R. M., Stansfeld, P. J., Dalibalta, S., Sutcliffe, M. J., and Mitcheson, J. S. (2007) Activation gating of hERG potassium channels: S6 glycines are not required as gating hinges. *J. Biol. Chem.* **282,** 31972–31981
41. Wang, R., Bolstad, J., Kong, H., Zhang, L., Brown, C., and Chen, S. R. (2004) The predicted TM10 transmembrane sequence of the cardiac Ca^{2+}-release channel (ryanodine receptor) is crucial for channel activation and gating. *J. Biol. Chem.* **279,** 3635–3642
42. Lyu, P. C., Sherman, J. C., Chen, A., and Kallenbach, N. R. (1991) Alpha-helix stabilization by natural and unnatural amino acids with alkyl side chains. *Proc. Natl. Acad. Sci. U.S.A.* **88,** 5317–5320